Microchimica Acta (2022) 189: 256
https://doi.org/10.1007/s00604-022-05354-x

ORIGINAL PAPER

Magnetic supercluster particles for highly sensitive magnetic biosensing of proteins

Songeun Kim[1,2] · Junyoung Kim[3,4] · Jisoo Im[1,2] · Minah Kim[3,4] · Taehyeong Kim[3,4] · Shan X. Wang[5,6] · Dokyoon Kim[3,4] · Jung-Rok Lee[1,2]

Received: 17 March 2022 / Accepted: 30 May 2022 / Published online: 14 June 2022

Abstract

A strategy is reported to improve the detection limits of current giant magnetoresistance (GMR) biosensors by augmenting the effective magnetic moment that the magnetic tags on the biosensors can exert. Magnetic supercluster particles (MSPs), each of which consists of ~ 1000 superparamagnetic cores, are prepared by a wet-chemical technique and are utilized to improve the limit of detection of GMR biosensors down to 17.6 zmol for biotin as a target molecule. This value is more than four orders of magnitude lower than that of the conventional colorimetric assay performed using the same set of reagents except for the signal transducer. The applicability of MSPs in immunoassay is further demonstrated by simultaneously detecting vascular endothelial growth factor (VEGF) and C-reactive protein (CRP) in a duplex assay format. MSPs outperform commercially available magnetic nanoparticles in terms of signal intensity and detection limit.

Keywords Magnetic nanoparticles · Giant magnetoresistance · Biosensors · Supercluster particles · Immunoassay

Introduction

Molecular diagnostic tools are required to have a superior sensitivity to detect subtle changes in biomarkers, such as DNAs [1, 2], proteins [3, 4], and metabolites [5], for effective disease diagnosis and drug evaluation. However, the detection of proteins has suffered from low sensitivity, and their amplification prior to detection is also technically very difficult. The importance of highly sensitive detection of proteins can be seen in many clinical situations. For example, early tumors release only extremely small amounts of tumor-specific antigens into the bloodstream [6, 7], whereas their timely detection is critical to improving the survival rate of the patients [8]. It has also been reported that virus antigen tests such as those for the spike proteins of SARS-CoV-2 are suited as a first-line test to screen people before further performing standard polymerase chain reaction (PCR)-based tests [9], where more sensitive detection of virus antigens can contribute more to identifying and separating the infected individuals.

Tremendous efforts have been made to enhance the sensitivity of optical biosensors [10, 11]. For instance, in lieu of enzyme-based colorimeters, fluorescent tags including quantum dots have been utilized to further push the limit of detection in optical biosensing [12, 13]. It has also been reported that the introduction of a gold layer or nanostructure in optical biosensors can amplify the signals via the surface plasmon resonance effect [11, 14], through which, for example, a detection limit as low as 2 pmol was recently achieved for biotin [15]. Furthermore, other types of biosensors based on different sensing mechanisms have been developed to achieve higher sensitivities than optical biosensors [3, 16]. Electrochemical biosensors that can utilize simple

✉ Dokyoon Kim
kimdk@hanyang.ac.kr

✉ Jung-Rok Lee
jungrok@ewha.ac.kr

1 Division of Mechanical and Biomedical Engineering, Ewha Womans University, Seoul 03760, Republic of Korea

2 Graduate Program in Smart Factory, Ewha Womans University, Seoul 03760, Republic of Korea

3 Department of Bionano Engineering and Bionanotechnology, Hanyang University, Ansan 15588, Republic of Korea

4 Center for Bionano Intelligence Education and Research, Hanyang University, Ansan 15588, Republic of Korea

5 Department of Materials Science and Engineering, Stanford University, Stanford, CA 94305, USA

6 Department of Electrical Engineering, Stanford University, Stanford, CA 94305, USA

sensor geometry without using bulky optical components are one of such examples and present a readiness for point-of-care (POC) tests, as demonstrated for CRP and biotin with detection limits of 3.3 pg mL^{-1} and 0.3 fmol, respectively [17, 18]. However, their signals are heavily affected by the pH and salinity of the samples and buffers, requiring extra endeavor to compensate for those effects [19].

Magnetic biosensors have been reported to be among the most sensitive devices owing to the lack of magnetic contents in biological samples in general, thereby capable of producing a very low background noise [20, 21]. Their sensitivities can be tailored by modifying the structure and geometry of the sensors and employing signal transduction tags such as magnetic nanoparticles, magnetic microbeads, or any other magnetic materials. By taking advantage of these aspects, magnetic biosensors have successfully been used in various applications including antibody monitoring [22–24], evaluation of protein–protein interactions [25, 26], DNA mutation measurement [27], and cancer biomarker detection [28, 29]. To further increase the sensitivity of magnetic biosensors, signal-generating tags are worth improving because magnetic biosensors typically detect the magnetic field from the tags attached to the target analytes rather than directly detecting the analytes themselves.

Superparamagnetic iron oxide nanoparticles (SPIONs) are one of the most frequently applied magnetic tags in biosensing because of their relatively cost-effective synthesis and facile surface functionalization [30]. However, their intrinsically small magnetic moment has limited the sensitive detection of target analytes, which in part prevents the widespread use of magnetic biosensors for medical diagnosis. It has been known that clustering SPIONs into a single-particle form can increase the magnetic responsiveness of the nanoparticles as an aggregate [31], and the application of such particles as T_2 contrast enhancement agents in magnetic resonance imaging has also been demonstrated [32, 33]. However, their utility in magnetic biosensors has not extensively been investigated so far, despite the assured advantage in signal transduction. Moreover, given that previously reported magnetic cluster particles mostly relied on rather loosely assembled structures of SPIONs [32–34], it is anticipated that the use of magnetic cluster particles with a high packing density would be able to push the limits of current magnetic biosensors even further.

In this regard, we herein report MSPs, wherein SPIONs are assembled with a close-packed structure to maximize their magnetic moment per particle, and their application in GMR biosensors. These particles show an outstanding ability to improve the detection limit of GMR biosensors compared to conventional optical assays. In addition, MSPs are capable of producing even higher magnetic signals in GMR biosensors than commercially available magnetic nanoparticles (MNPs) can do, thereby allowing more sensitive detection of protein biomarkers as demonstrated for VEGF and CRP.

Materials and methods

Materials and instruments

All organic solvents and buffer solutions are prepared with analytical grade reagents. Phosphate-buffered saline (PBS) at pH 7.4 and borate buffer at pH 8.0 was purchased from Thermo Fisher and Sigma-Aldrich, respectively. Capture and detection antibodies for human VEGF and CRP were purchased from R&D systems. Commercially available chemical compounds were used for synthesizing nanoparticles and performing assays. TEM images were obtained using JEM-2100F (JEOL, Japan) at 200 kV. Hydrodynamic sizes of MSPs were analyzed using Zetasizer Nano-ZS (Malvern, UK). Magnetization curves of SPIONs and MSPs were obtained using PPMS-14 (Quantum Design, USA). The immobilization of probes onto the GMR biosensors was performed with a non-contact robotic arrayer, SciFlexArrayer S3 (Scienion, Germany). GMR signals were obtained using a custom-made reader system, as described previously [21, 35]. For sensitivity comparison, streptavidin-MNPs were purchased from Miltenyi Biotec (Germany).

Fabrication of SPIONs

Iron(III) oleate was made using a method slightly modified from a previous report [36] (see detailed protocols in Supplementary Information). To produce 19-nm-sized SPIONs, iron(III) oleate (1.8 g) was heated with 1-octadecene (10 g) and oleic acid (0.3 g) for 30 min at 320 °C under vigorous stirring. Then, the resultant solution was cooled down and washed with excess ethanol. SPIONs were separated by precipitation via centrifugation (5000 rpm, 30 min). The collected SPIONs were washed and centrifuged twice more.

Synthesis of MSPs

MSPs are produced by assembling pre-synthesized SPIONs of a uniform size through a microemulsion-based process (Fig. 1). Briefly, 19-nm-sized SPIONs were dispersed in chloroform (3 mL) at a concentration of 50 mg mL^{-1}. Dodecyltrimethylammonium bromide (DTAB) dissolved in deionized water (10 mL) at 15 mg mL^{-1} was then added to the chloroform solution. The mixture solution was stirred vigorously for 12 h to evaporate the chloroform. The hydrophobic interactions between the surface capping ligands on the SPIONs and DTAB in water resulted in the close packing of the SPIONs in each MSP. Then, poly(acrylic acid) (PAA) ($M_w = 1800$) dissolved in ethylene glycol (10 mL) at

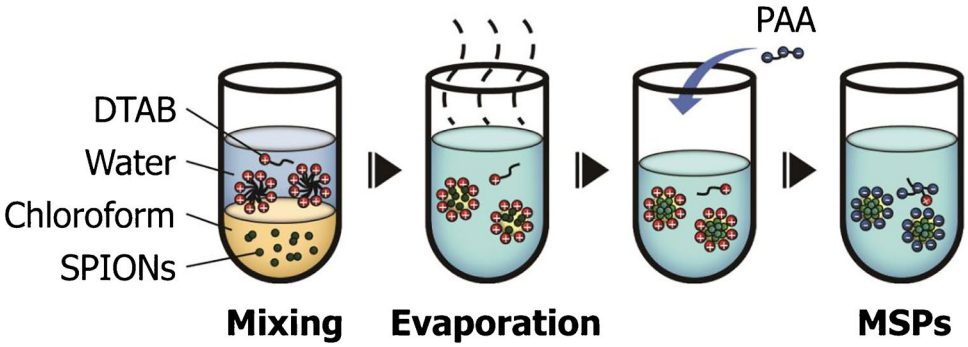

Fig. 1 Schematic of MSP formation. SPIONs are emulsified with an aqueous solution of DTAB, assembled into an ordered structure by evaporating chloroform, and coated with PAA

100 mg mL^{-1} was added. This subsequent coating with PAA further improved the colloidal stability of MSPs and provided the functional groups for streptavidin conjugation. The MSPs in the solution were washed with excess deionized water and separated by centrifugation (5000 rpm, 5 min).

Fabrication of streptavidin-MSPs

MSPs (1 mg [Fe]) dispersed in deionized water (0.5 mL) was mixed with 1-ethyl-3-(3-(dimethylamino)propyl)urea hydrochloride and N-hydroxysuccinimide at 10 mg mL^{-1} each in 2-(N-morpholino)ethanesulfonic acid buffer (0.1 mL) for 30 min. The MSPs were separated by centrifugation (5000 rpm, 5 min) and reacted for 1 h with streptavidin (0.1 mg) in PBS (1 mL). The streptavidin-MSPs were washed with excess borate buffer and separated by centrifugation (5000 rpm, 5 min).

GMR biosensor sensitivity test

A 10 × 8 array of GMR biosensors (100 × 100 µm, each) was fabricated on a chip (5 × 4 mm), mounted on a printed circuit board and assembled with a custom-designed cartridge to create a reaction well over the sensors. The GMR biosensors with a temperature correction feature consist of multiple stripes of spin-valve stacks, as described previously [35, 37]. Briefly, thin films of seed layer/IrMn (8)/CoFe (2)/Ru (0.8)/CoFe (2)/Cu (2.3)/CoFe (4.5) (all thicknesses in nm) were fabricated on a Si/SiO_2 substrate. The capping layer at the top of this structure protects the sensors from stringent conditions and ensures the pH- and salinity-insensitive operation of the sensors [20, 25]. For estimating the limit of detection, approximately 2 nL of solutions containing 1% bovine serum albumin (BSA) or biotinylated BSA (biotin-BSA) ranging from 35 zmol to 35 fmol were spotted on different GMR biosensors with replicates, respectively, using a non-contact robotic arrayer. After overnight incubation of the sensor chip in a humid chamber at 4 °C, the chip was washed with a washing buffer (PBS with 0.1% BSA and 0.05% Tween-20) and then incubated with 1% BSA in PBS for 1 h. The chip was washed again with the washing buffer and inserted into a custom-made reader system. After obtaining the baseline signals from the sensors, 60 µL of MSP solution diluted 10 times with borate buffer was added to the reaction well and incubated for 40 min while the signals were being recorded. Then, the chip was carefully washed with the washing buffer, and the signals were obtained for the subsequent analyses. For comparison with enzyme-linked immunosorbent assay (ELISA), a microplate containing the same amounts of samples with replicates was prepared following the general ELISA protocols. The limit of detection was determined as the level two times the standard deviation above the zero-analyte signal.

GMR biosensor immunoassays

For immunoassays, anti-VEGF capture antibodies and anti-CRP capture antibodies at 0.5 mg mL^{-1} each were spotted on different sensors with replicates along with BSA as a negative control, using the arrayer. The chip was incubated overnight, washed with the washing buffer, and then incubated with 1% BSA in PBS for 1 h, as described above. A mixture of VEGF and CRP at indicated concentrations was added to a set of two identically prepared chips, respectively, and incubated for 1 h. The chips were again washed with the washing buffer, and a mixture of anti-VEGF detection antibodies and anti-CRP detection antibodies at 0.5 µg mL^{-1} each was added to the chips and incubated for 1 h. Washed with the washing buffer, the chips were inserted into the reader system. After obtaining the baseline signals, 60 µL of the commercially available streptavidin-MNPs or the prepared streptavidin-MSPs was introduced to each chip for signal comparison.

Results and discussion

Characterization of MSPs

SPIONs are synthesized by thermally decomposing iron(III) oleate in 1-octadecene as a non-coordinating solvent. Oleic acid is used as a surface capping ligand to regulate the size

distribution of SPIONs tightly during the synthesis. The size of SPIONs is verifiable in the transmission electron microscope (TEM) image that shows an average diameter of ~ 19 nm (Fig. 2a and Supplementary Information Fig. S1). X-ray diffraction (XRD) analysis reveals a cubic spinel-structured Fe_3O_4 phase of the SPIONs (Fig. 2b). Because the SPIONs are smaller than the superparamagnetic limit size of Fe_3O_4 [38], they are expected to be superparamagnetic.

The uniformity in size of the constituent SPIONs is evident from the formation of the ordered superlattice in the MSPs as shown in the TEM image (Fig. 3a). The average size of the produced MSPs is ~ 190 nm. By assuming a hard-sphere model of close-packed 19-nm-sized SPIONs, a 190-nm-sized MSP is estimated to consist of approximately ~ 1000 SPIONs. The magnetization curve obtained for the MSPs at 300 K displays a superparamagnetic behavior with no remanent magnetization at zero fields (Fig. 3b), implying that the superparamagnetic property of SPIONs is preserved in MSPs. Although the saturation magnetization of MSPs is only ~ 23% larger than that of SPIONs in terms of mass, it is evident that MSPs exhibit a very large magnetization per particle due to its assembly structure made of ~ 1000 SPIONs. The hydrodynamic size of MSPs measured by dynamic light scattering (DLS) shows an intense peak at 202 nm (Fig. 3c) which is close to the size observed by TEM analysis (Fig. 3a). To use MSPs as magnetic tags in biosensing, streptavidin is immobilized onto the MSP surface via the conjugation between the carboxylic acid groups in PAA and the amine groups in streptavidin. DLS measurement data shows a concomitant increase in the hydrodynamic size of MSPs after the functionalization with streptavidin (Fig. 3c). The resulting streptavidin-MSPs are capable of binding to biotin and biotinylated proteins because of the very high affinity between streptavidin and biotin.

The limit of detection with GMR biosensors using MSPs

To figure out the limit of detection using MSPs on GMR biosensors shown in Fig. 4a, different concentrations of biotin-BSA are immobilized on the sensors with replicates. In parallel, the same amounts of biotin-BSA are added into ELISA microplate wells for comparison. The main feature of the GMR biosensor compared with the conventional colorimetric sandwich immunoassays is the use of magnetic tags as a signal transducer. After the application of

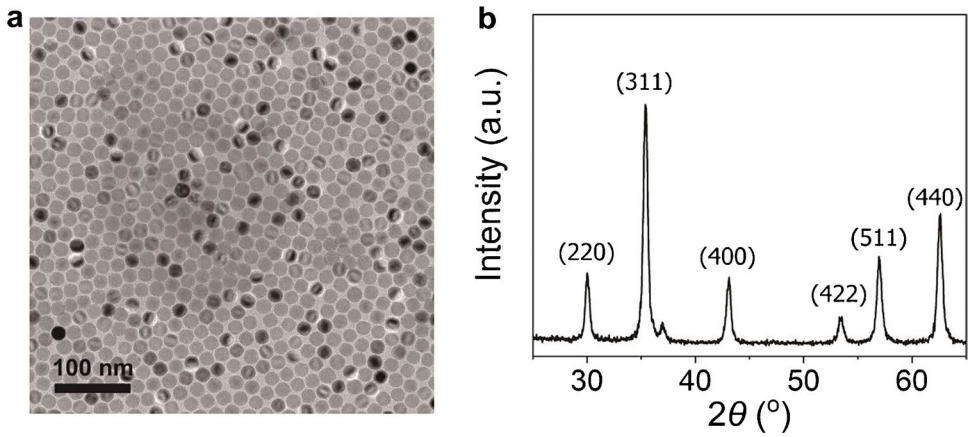

Fig. 2 **a** TEM image of SPIONs. The scale bar is 100 nm. **b** X-ray diffraction pattern of SPIONs

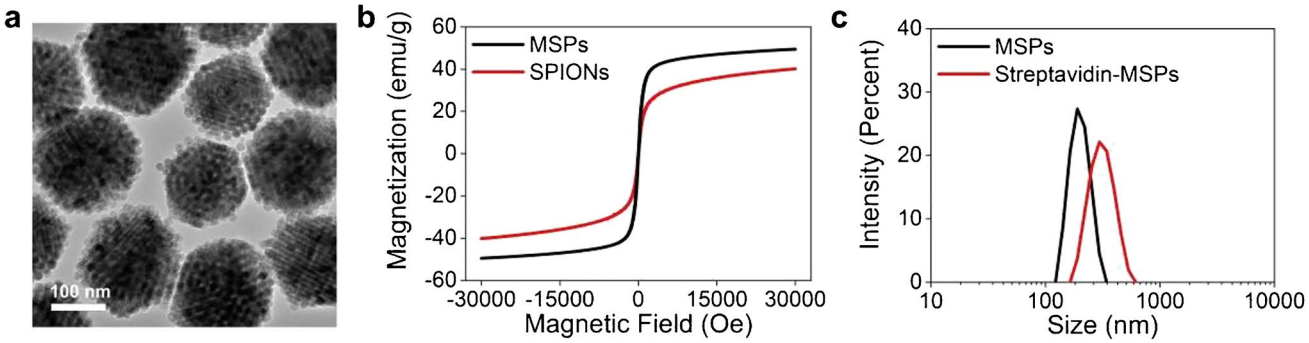

Fig. 3 Characterization of MSPs. **a** TEM image of MSPs. The scale bar is 100 nm. **b** Magnetization curve of MSPs (black) and SPIONs (red). **c** Hydrodynamic sizes of MSPs measured before and after conjugation of streptavidin

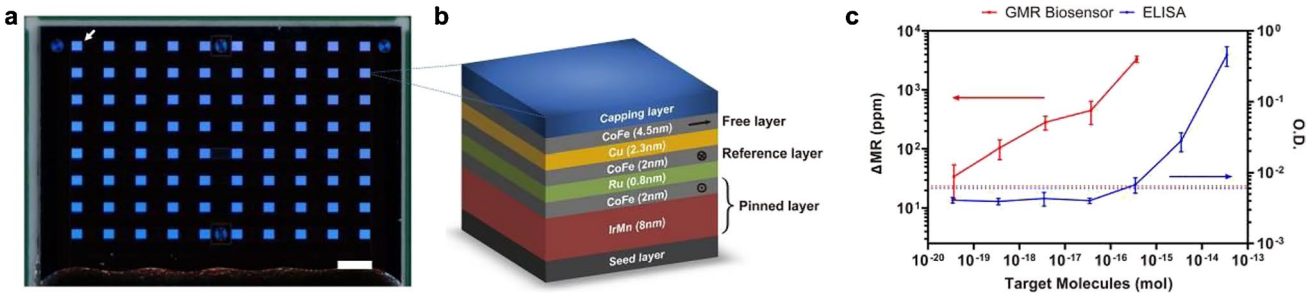

Fig. 4 GMR biosensors and titration curves for biotin-BSA. **a** Optical image of a GMR biosensor chip consisting of 80 sensors. A white arrow indicates an individual sensor. The scale bar is 500 µm. **b** Structure of the spin-valve stack (not to scale). **c** Titration curves of GMR biosensor (red line) and direct ELISA (blue line) measurements. Error bars are standard deviations ($n = 3$). The dotted lines indicate the average plus two standard deviations of the signals from BSA-coated GMR biosensors (red) and ELISA wells (blue), respectively

an external magnetic field, stray magnetic fields are generated as a response to the magnetic tags bound on the sensor surface, such that they enhance the effective magnetic field that the GMR biosensor experiences [37]. Since the external magnetic field is applied in a way to misalign the magnetization directions of the magnetic free and reference layers of the spin-valve stack (Fig. 4b), the added field strength by the magnetic tags eventually leads to more misalignment between those two layers. When a voltage is applied to the GMR biosensor, the conducting electrons are supposed to exhibit a spin-dependent scattering behavior while passing through the copper layer positioned in between the magnetic free and reference layers. Such a spin-dependent scattering is proportional to the degree of the misalignment. In other words, the change in the magnetoresistance (ΔMR) of the GMR biosensor is affected by the number of magnetic tags bound on the biosensor surface and thus the concentration of the target analyte. In both experiments, biotin-BSA is used as the target analyte to directly capture the signal transducers in both modalities, to minimize the chances of target unbinding, and to more accurately estimate the number of target molecules on the surface. Thus, we add streptavidin-MSPs to the GMR biosensors and streptavidin–horseradish peroxidase (streptavidin-HRP) to the ELISA wells to obtain the signals. The optical density at 450 nm is measured for ELISA using a microplate reader, and the data shown in Fig. 4c indicate that the limit of detection in ELISA is approximately 0.1 fmol, which is consistent with the previously reported values [20]. The detection limit of the GMR biosensors in combination with streptavidin-MSPs is estimated to be 17.5 zmol, which is more than four orders of magnitude lower than that of ELISA (490 amol).

Duplex immunoassay with GMR biosensors

After confirming the high performance of streptavidin-MSPs as a signal transducer for GMR biosensors, this combination is further evaluated against the combination with commercially available streptavidin-MNPs to demonstrate the higher detection sensitivity of streptavidin-MSPs in protein immunoassay. Figure 5a–e schematically illustrate the procedures of the sandwich immunoassay based on GMR biosensors using streptavindin-MSPs. Specifically, different sensors on the GMR biosensor chip are functionalized with either capture antibody or BSA, where the latter serves as a negative control. Then, the samples and the corresponding detection antibodies are added, washed, and incubated sequentially to form the sandwich structure. Two kinds of protein biomarkers, VEGF and CRP, are tested in a multiplexed way after verifying the absence of cross-reactivity between them (Supplementary Information Fig. S2). VEGF is a mediator of cancerous angiogenesis and is found to be at high levels in tumors [39]. CRP is produced mainly in response to inflammation, thus related to many morbid conditions including cancer, autoimmune diseases, and health problems [40, 41]. A mixture of VEGF and CRP both at 0.005, 0.025, 0.125 or 0.625 ng mL^{-1} is incubated with two identically processed chips, but each chip is assayed with either streptavidin-MSPs or streptavidin-MNPs for comparison. When streptavidin-MSPs are employed to bind to the biotinylated detection antibodies, signals proportional to the target analyte concentrations are obtained as expected (Fig. 5f). Importantly, the signals produced by streptavidin-MSPs are much greater than the signals produced by the commercially available streptavidin-MNPs (Fig. 5g). This signal enhancement is reasoned to the much larger number of magnetic SPIONs incorporated in MSPs than in MNPs, as can be verified by their TEM images (Fig. 3a and Supplementary Information Fig. S3) and thus the corresponding increase in the magnetic moment per particle. As a result, the limits of detection for VEGF and CRP using MSPs are 1.4 and 9.0 pg mL^{-1}, respectively, which are lower than the detection limits by MNPs (50 and

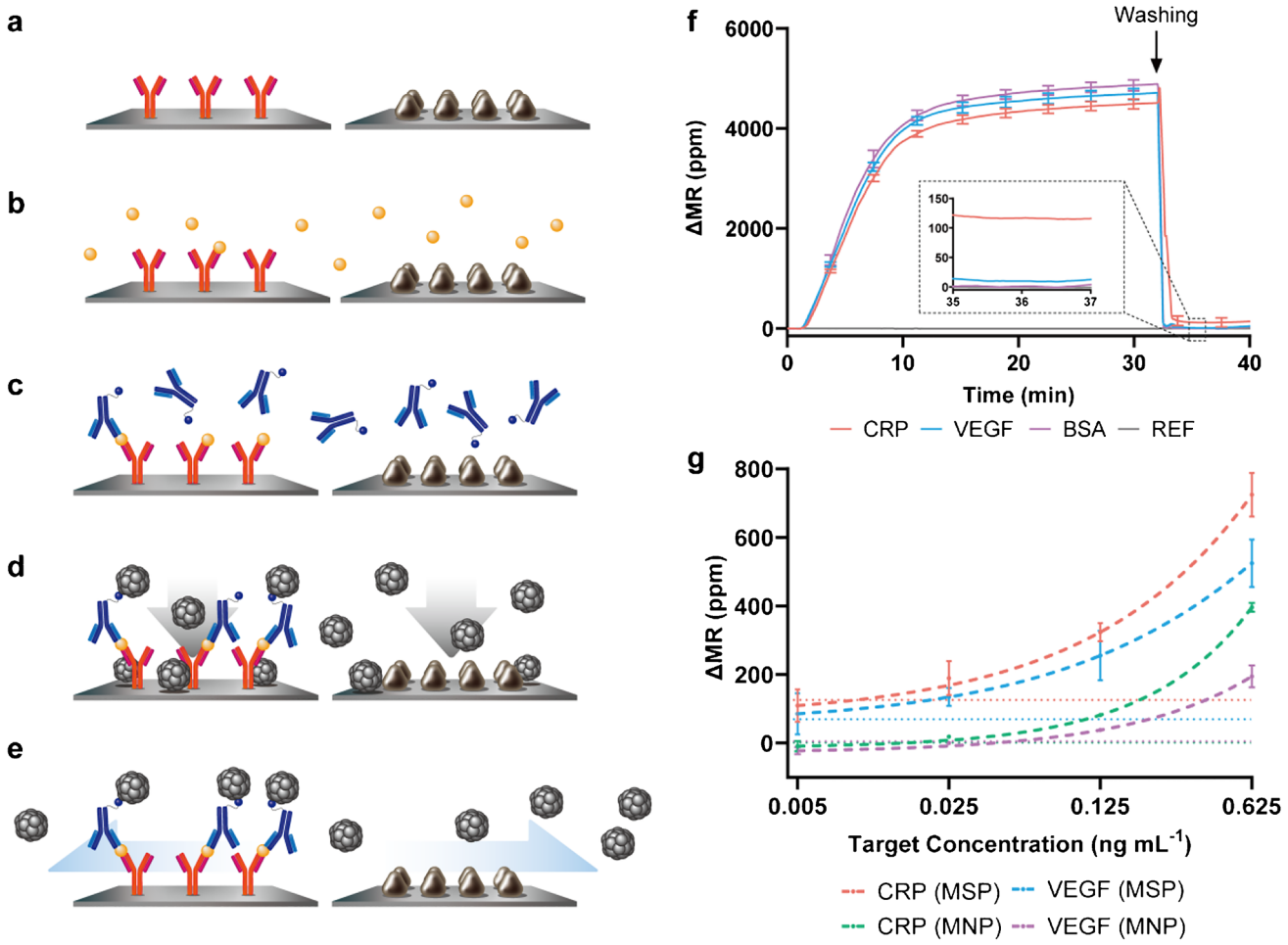

Fig. 5 Detection of protein analytes using GMR biosensors. **a**–**e** A schematic of the GMR biosensor immunoassay using streptavidin-MSPs. **a** Capture antibodies (left) and BSA (right) are immobilized on the surface of each sensor. Anti-VEGF and anti-CRP capture antibodies are immobilized on different sensors for multiplexed assays. **b** Target analytes are added to the sensor chip and bound to the capture antibodies. No analyte is bound to BSA. **c** Biotinylated detection antibodies are introduced to the sensor chip and bound to the target analytes that are captured by the capture antibodies. **d** Streptavidin-MSPs are added and bound to the detection antibodies via the streptavidin–biotin interaction. **e** Unbound streptavidin-MSPs are removed through washing. **f** Typical real-time signals obtained from GMR biosensors. At about 1 min, streptavidin-MSPs are added to the chip, and washing was performed at 32 min. **g** Standard curves obtained by multiplexed measurements of VEGF and CRP after application of streptavidin-MSPs or streptavidin-MNPs. The dotted lines indicate the average plus two standard deviations of the zero analyte signals. Error bars are standard deviations ($n = 4$)

16.5 pg mL^{-1}). These sensitive measurements with MSPs perform better than conventional ELISA (Supplementary Information Fig. S4).

Conclusions

MSPs were developed to circumvent the inherent limitation of SPIONs as magnetic tags. The unique structure of MSPs with a very high loading density of SPIONs not only contributes to preserving their superparamagnetic property but also greatly improves their capability to generate signals on GMR biosensors, as shown by using biotin-BSA as the target analyte. Furthermore, in our demonstration of a multiplexed immunoassay for VEGF and CRP, streptavidin-MSPs outperform the commercial streptavidin-MNPs, which contain only a few loosely coalesced SPIONs, in terms of the signal generation. A drawback of the MSP-based magnetic immunoassay demonstrated in this study would be the necessity of a washing step for the end-point measurement. However, we believe that the significant improvement in magnetic signal transduction achievable by MSPs still provides a meaningful advantage over the inconvenience due to the additional washing process, especially for the cases where high sensitivities are extremely desired. Moreover, such a procedure can easily be implemented if the sensor system is integrated within a microfluidic chip [42]. Since the surface functionalization of MSPs is compatible with

the conventional immunoassay procedures and relies on the specific antigen–antibody interactions, MSPs would be able to find their appropriate use in various types of magnetic sensing platforms for biomedical research and diagnosis.

Supplementary Information The online version contains supplementary material available at https://doi.org/10.1007/s00604-022-05354-x.

CRediT authorship contribution statement Songeun Kim: validation, formal analysis, visualization; Junyoung Kim: synthesis; Jisoo Im: validation; Minah Kim: synthesis; Taehyeong Kim: characterization; Shan X. Wang: resources, writing—review and editing; Dokyoon Kim: conceptualization, formal analysis, investigation, writing—original draft; Jung-Rok Lee: supervision, resources, writing—review and editing.

Funding This work was supported by the National Research Foundation of Korea (NRF) grant funded by the Korean government (NRF-2018R1A6A1A03024231, NRF-2018R1D1A1B07050979, NRF-2019M3C1B8090804, NRF-2020R1C1C1005416, NRF-2022R1A2C1003527). S.X.W. acknowledges support from the National Institutes of Health (NIH) grant R01CA25784301.

Declarations

Conflict of interest S.X.W. has related patents or patent applications assigned to Stanford University and out-licensed for potential commercialization. S.X.W. has stock or stock options in MagArray, Inc., which has licensed relevant patents from Stanford University for the commercialization of GMR biosensor chips.

References

1. Myhrvold C, Freije CA, Gootenberg JS et al (2018) Field-deployable viral diagnostics using CRISPR-Cas13. Science 360(6387):444–448. https://doi.org/10.1126/science.aas8836
2. Huang RR, He NY and Li ZY (2018) Recent progresses in DNA nanostructure-based biosensors for detection of tumor markers. BiosensBioelectron 10927-34. https://doi.org/10.1016/j.bios.2018.02.053
3. Wu GH, Datar RH, Hansen KM et al (2001) Bioassay of prostate-specific antigen (PSA) using microcantilevers. Nat Biotechnol 19(9):856–860. https://doi.org/10.1038/nbt0901-856
4. Wang ZY, Luan JY, Seth A et al (2021) Microneedle patch for the ultrasensitive quantification of protein biomarkers in interstitial fluid. Nat Biomed Eng 5(1):64–76. https://doi.org/10.1038/s41551-020-00672-y
5. Kim J, Campbell AS, de Avila BEF et al (2019) Wearable biosensors for healthcare monitoring. Nat Biotechnol 37(4):389–406. https://doi.org/10.1038/s41587-019-0045-y
6. Hori SS, Gambhir SS (2011) Mathematical model identifies blood biomarker-based early cancer detection strategies and limitations. Sci Transl Med 3(109):109ra116. https://doi.org/10.1126/scitranslmed.3003110
7. Lutz AM, Willmann JK, Cochran FV et al (2008) Cancer screening: a mathematical model relating secreted blood biomarker levels to tumor sizes. Plos Med 5(8):1287–1297. https://doi.org/10.1371/journal.pmed.0050170
8. Siegel RL, Miller KD, Fuchs HE et al (2022) (2022) Cancer statistics. Ca-Cancer J Clin 72(1):7–33. https://doi.org/10.3322/caac.21708
9. Scohy A, Anantharajah A, Bodeus M et al (2020) Low performance of rapid antigen detection test as frontline testing for COVID-19 diagnosis. J Clin Virol 129:104455. https://doi.org/10.1016/j.jcv.2020.104455
10. Fan XD, White IM, Shopova SI et al (2008) Sensitive optical biosensors for unlabeled targets: a review. Anal Chim Acta 620(1–2):8–26. https://doi.org/10.1016/j.aca.2008.05.022
11. Cathcart N, Chen JIL (2020) Sensing Biomarkers with Plasmonics. Anal Chem 92(11):7373–7381. https://doi.org/10.1021/acs.analchem.0c00711
12. Algar WR, Tavares AJ, Krull UJ (2010) Beyond labels: a review of the application of quantum dots as integrated components of assays, bioprobes, and biosensors utilizing optical transduction. Anal Chim Acta 673(1):1–25. https://doi.org/10.1016/j.aca.2010.05.026
13. Wegner KD, Hildebrandt N (2015) Quantum dots: bright and versatile in vitro and in vivo fluorescence imaging biosensors. Chem Soc Rev 44(14):4792–4834. https://doi.org/10.1039/c4cs00532e
14. Huang CJ, Ye J, Wang S et al (2012) Gold nanoring as a sensitive plasmonic biosensor for on-chip DNA detection. Appl Phys Lett 100(17):173114. https://doi.org/10.1063/1.4707382
15. Lin WZ, Chen YH, Liang CK et al (2019) A competitive immunoassay for biotin detection using magnetic beads and gold nanoparticle probes. Food Chem 271:440–444. https://doi.org/10.1016/j.foodchem.2018.07.152
16. Sadighbayan D, Sadighbayan K, Khosroushahi AY et al (2019) Recent advances on the DNA-based electrochemical biosensing of cancer biomarkers: analytical approach. Trac-Trend Anal Chem 119:115609. https://doi.org/10.1016/j.trac.2019.07.020
17. Ma YC, Yang J, Yang T et al (2020) Electrochemical detection of C-reactive protein using functionalized iridium nanoparticles/graphene oxide as a tag. Rsc Adv 10(16):9723–9729. https://doi.org/10.1039/c9ra10386d
18. Buyuktiryaki S, Yazici B, Ersoz A et al (2022) Application of HRP-streptavidin bionanoparticles for potentiometric biotin determination. Bioelectrochemistry 144:107993. https://doi.org/10.1016/j.bioelechem.2021.107993
19. Wu CC, Wang MR (2021) Effects of buffer concentration on the sensitivity of silicon nanobelt field-effect transistor sensors. Sensors-Basel 21(14):4904. https://doi.org/10.3390/s21144904
20. Gaster RS, Hall DA, Nielsen CH et al (2009) Matrix-insensitive protein assays push the limits of biosensors in medicine. Nat Med 15(11):1327–1332. https://doi.org/10.1038/nm.2032
21. Hall DA, Gaster RS, Lin T et al (2010) GMR biosensor arrays: a system perspective. Biosens Bioelectron 25(9):2051–2057. https://doi.org/10.1016/j.bios.2010.01.038
22. Lee JR, Haddon DJ, Gupta N et al (2016) High-resolution analysis of antibodies to post-translational modifications using peptide nanosensor microarrays. ACS Nano 10(12):10652–10660. https://doi.org/10.1021/acsnano.6b03786
23. Xu LY, Lee JR, Hao SY et al (2019) Improved detection of prostate cancer using a magneto-nanosensor assay for serum circulating autoantibodies. PLoS ONE 14(8):e0221051. https://doi.org/10.1371/journal.pone.0221051
24. Lee JR, Chan CT, Ruderman D et al (2017) Longitudinal monitoring of antibody responses against tumor cells using magneto-nanosensors with a nanoliter of blood. Nano Lett 17(11):6644–6652. https://doi.org/10.1021/acs.nanolett.7b02591
25. Lee JR, Bechstein DJB, Ooi CC et al (2016) Magneto-nanosensor platform for probing low-affinity protein-protein interactions and identification of a low-affinity PD-L1/PD-L2 interaction. Nat Commun 7:12220. https://doi.org/10.1038/ncomms12220
26. Roth S, Zander I, Michelson Y et al (2020) Identification of protein-protein interactions using a magnetic modulation biosensing system. Sensor Actuat B-Chem 303:127228. https://doi.org/10.1016/j.snb.2019.127228

27. Rizzi G, Osterberg FW, Dufva M et al (2014) Magnetoresistive sensor for real-time single nucleotide polymorphism genotyping. Biosens Bioelectron 52:445–451. https://doi.org/10.1016/j.bios.2013.09.026
28. Khramtsov P, Kropaneva M, Bochkova M et al (2019) Solid-phase nuclear magnetic resonance immunoassay for the prostate-specific antigen by using protein-coated magnetic nanoparticles. Microchim Acta 186(12):768. https://doi.org/10.1007/s00604-019-3925-4
29. Lee JR, Appelmann I, Miething C et al (2018) Longitudinal multiplexed measurement of quantitative proteomic signatures in mouse lymphoma models using magneto-nanosensors. Theranostics 8(5):1389–1398. https://doi.org/10.7150/thno.20706
30. Rocha-Santos TAP (2014) Sensors and biosensors based on magnetic nanoparticles. Trac-Trend Anal Chem 62:28–36. https://doi.org/10.1016/j.trac.2014.06.016
31. Hong H, Min SH, Koo S et al (2022) Dynamic ligand screening by magnetic nanoassembly modulates stem cell differentiation. Adv Mater 34(2):2105460. https://doi.org/10.1002/adma.202105460
32. Li FY, Liang ZY, Liu JN et al (2019) Dynamically reversible iron oxide nanoparticle assemblies for targeted amplification of T1-weighted magnetic resonance imaging of tumors. Nano Lett 19(7):4213–4220. https://doi.org/10.1021/acs.nanolett.8b04411
33. Cai ZY, Wu CQ, Yang L et al (2020) Assembly-controlled magnetic nanoparticle clusters as MRI contrast agents. Acs Biomater Sci Eng 6(5):2533–2542. https://doi.org/10.1021/acsbiomaterials.9b01198
34. Yoon TJ, Lee H, Shao HL et al (2011) Multicore assemblies potentiate magnetic properties of biomagnetic nanoparticles. Adv Mater 23(41):4793–4797. https://doi.org/10.1002/adma.201102948
35. Hall DA, Gaster RS, Osterfeld SJ et al (2010) GMR biosensor arrays: correction techniques for reproducibility and enhanced sensitivity. Biosens Bioelectron 25(9):2177–2181. https://doi.org/10.1016/j.bios.2010.01.039
36. Park J, An KJ, Hwang YS et al (2004) Ultra-large-scale syntheses of monodisperse nanocrystals. Nat Mater 3(12):891–895. https://doi.org/10.1038/nmat1251
37. Lee JR, Sato N, Bechstein DJB et al (2016) Experimental and theoretical investigation of the precise transduction mechanism in giant magnetoresistive biosensors. Sci Rep 6:18692. https://doi.org/10.1038/srep18692
38. Kim D, Lee N, Park M et al (2009) Synthesis of uniform ferrimagnetic magnetite nanocubes. J Am Chem Soc 131(2):454–455. https://doi.org/10.1021/ja8086906
39. Syedmoradi L, Ahmadi A, Norton ML et al (2019) A review on nanomaterial-based field effect transistor technology for biomarker detection. Microchim Acta 186(11):739. https://doi.org/10.1007/s00604-019-3850-6
40. Liu TZ, Hu R, Liu Y et al (2020) Amperometric immunosensor based on covalent organic frameworks and Pt/Ru/C nanoparticles for the quantification of C-reactive protein. Microchim Acta 187(6):320. https://doi.org/10.1007/s00604-020-04286-8
41. Alba-Patino A, Vaquer A, Baron E et al (2022) Micro- and nanosensors for detecting blood pathogens and biomarkers at different points of sepsis care. Microchim Acta 189(2):74. https://doi.org/10.1007/s00604-022-05171-2
42. Bechstein DJB, Lee JR, Ooi CC et al (2015) High performance wash-free magnetic bioassays through microfluidically enhanced particle specificity. Sci Rep 5:11693. https://doi.org/10.1038/srep11693